Correlating Non-Geminate Recombination with Film Structure: A Comparison of Polythiophene: Fullerene Bilayer and Blend Films

ARTICLE *in* JOURNAL OF PHYSICAL CHEMISTRY LETTERS · NOVEMBER 2014

Impact Factor: 7.46 · DOI: 10.1021/jz5018575

8 AUTHORS, INCLUDING:

Safa Shoaee
Imperial College London
27 PUBLICATIONS **669** CITATIONS
SEE PROFILE

Donal D. C. Bradley
University of Oxford
661 PUBLICATIONS **46,047** CITATIONS
SEE PROFILE

Veaceslav Coropceanu
Georgia Institute of Technology
125 PUBLICATIONS **7,424** CITATIONS
SEE PROFILE

Thomas Anthopoulos
Imperial College London
227 PUBLICATIONS **7,459** CITATIONS
SEE PROFILE

THE JOURNAL OF PHYSICAL CHEMISTRY Letters

Letter

pubs.acs.org/JPCL

Correlating Non-Geminate Recombination with Film Structure: A Comparison of Polythiophene: Fullerene Bilayer and Blend Films

Safa Shoaee,*[,†,∥] Shafigh Mehraeen,[‡] John G. Labram,[§] Jean-Luc Brédas,[‡] Donal D. C. Bradley,[§] Veaceslav Coropceanu,[‡] Thomas D. Anthopoulos,[§] and James R. Durrant*[,†]

[†]Centre for Plastic Electronics, Department of Chemistry, Imperial College London, London SW7 2AZ, United Kingdom

[‡]School of Chemistry and Biochemistry and Centre for Organic Photonics and Electronics, Georgia Institute of Technology, Atlanta, Georgia 30332-0400, United States

[§]Centre for Plastic Electronics, Department of Physics, Imperial College London, London SW7 2AZ, United Kingdom

Supporting Information

ABSTRACT: The morphology of the active layer in polymer:fullerene solar cells is a key parameter in determining their performance. In this study we monitor the charge carrier dynamics in bilayers of poly(3-hexylthiophene) (P3HT) and [6,6]-phenyl-C61-butyric acid methyl ester (PCBM) (fabricated by sequential spin coating and vacuum deposition) before and after thermal annealing, and compare these against conventional solution processed bulk heterojunction (BHJ) blend films. Transmission electron microscopy images, supported by field effect mobility data show that while not-annealed P3HT/$PC_{61}BM$ bilayers possess a sharp interface, intermixing proceeds upon annealing. Transient absorption studies indicate that the not-annealed bilayer yields fewer, but longer lived, charge carriers compared to the BHJ. Monte Carlo (MC) simulations further suggest that the difference in non-geminate recombination dynamics observed for the BHJ and bilayer films could be related to the confinement of charge carriers to the interface, with the lower dimensionality for the flat interface bilayer films relative to the intercalated donor−acceptor network BHJ films leading to lower recombination.

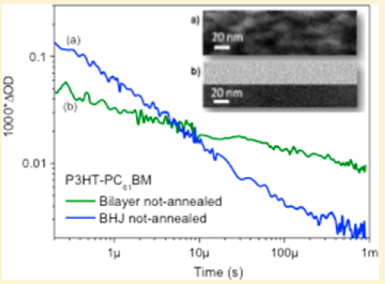

SECTION: Physical Processes in Nanomaterials and Nanostructures

As a promising alternative to inorganic photovoltaics, organic solar cells have developed rapidly in recent years. Organic photovoltaics (OPVs) are fabricated with either donor/acceptor bulk heterojunction (BHJ) or bilayer device architectures. A key consideration in the design of such devices is the impact of film structure upon device performance. In general, the use of BHJ film structures facilitates the diffusion of photogenerated excitons to the charge separation interface, as organic materials usually exhibit exciton diffusion lengths of ∼10 nm and 1/e optical absorption depths of ∼50−100 nm.[1] However, this more intimate mixing of donor and acceptor materials also increases the interfacial area available for the non-geminate recombination of charge carriers, and can therefore result in a reduced efficiency for the collection of photogenerated charge carriers by the device electrodes.

There is increasing evidence that non-geminate recombination is an important factor limiting device performance, and in particular device open circuit voltage.[2−5] While these considerations are generally accepted, relatively few studies to date have directly correlated experimental measurements of film micro/nanostructure with direct measurements of non-geminate recombination.[6,7] For example, most models of device photovoltaic performance, and particularly device open circuit voltage, are based upon consideration of materials energy levels alone, without explicit consideration of film structure.[8,9] The omission derives in part from the difficulty of measuring structural parameters of direct functional importance, and in part from an uncertainty as to how they quantitatively impact upon the underlying optoelectronic processes. In this regard, increasing attention is being placed on analyses of the structure of such blend films, and how this impacts upon device performance.[10−16] Blend film structure is also important for optical gain properties, with P3HT surprisingly efficient as a lasing medium when dispersed in a suitable host material.[17]

It is becoming apparent that structural models for polymer/fullerene blend films that comprise simple bicontinuous, interpenetrating donor and acceptor domains are inadequate to explain photovoltaic function. In this report, we employ transmission electron microscopy (TEM) alongside optical spectroscopy to probe specifically the correlation between nanostructure and recombination dynamics, employing a series of donor/acceptor films comprising a conventional polymer/fullerene BHJ structure and a polymer/fullerene bilayer fabricated with the same materials and studied both before and after thermal annealing. The experimental results are modeled using Kinetic Monte Carlo (KMC) simulations of charge recombination, allowing a consistent explanation of the

Received: September 3, 2014
Accepted: October 6, 2014
Published: October 6, 2014

   dx.doi.org/10.1021/jz5018575 | J. Phys. Chem. Lett. 2014, 5, 3669−3676

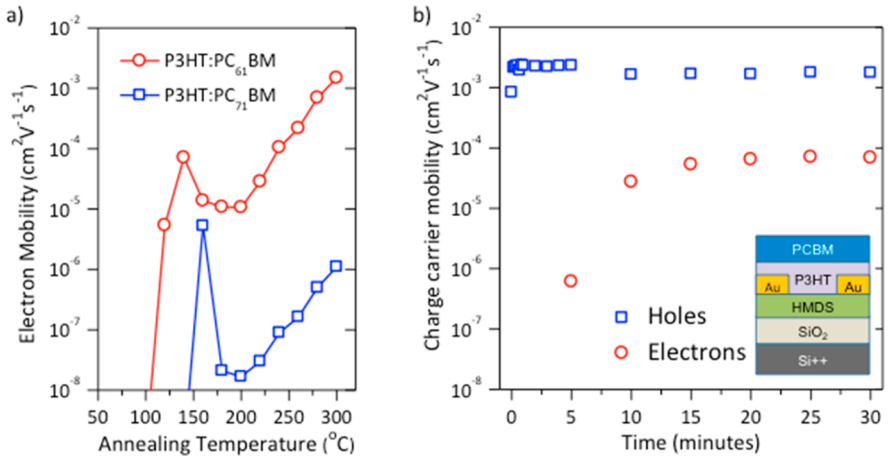

Figure 1. (a) Saturation-regime field-effect mobility of electrons in bilayer P3HT/$PC_{61}BM$ and P3HT/$PC_{71}BM$ organic field-effect transistors (OFETs) measured at room temperature under ambient-pressure N_2, after being annealed at various temperatures for 30 min. The length and width of the devices measured were 10 μm and 10 mm, respectively, in both cases. (b) Saturation-regime field-effect mobility of holes and electrons in bilayer P3HT/$PC_{71}BM$ OFET measured under ambient-pressure N_2 after being annealed at 160 °C, plotted as a function of time. The length and width of the device measured was 40 μm and 10 mm, respectively The thicknesses of the P3HT and PCBM layers were 8 and 40 nm, respectively, in the P3HT/PC61BM OFETs, and 25 and 25 nm, respectively, in the P3HT/PC71BM OFETs.[35,37] Inset: a schematic representation of the device architecture.

observed variations in charge yield and recombination dynamics.

For BHJ devices, it is clear that active layer film light absorption,[8] material energy levels,[18] and heterojunction nanostructure[19] are all important in determining device efficiency.[20] The first two factors can be addressed by molecular engineering through, for example, the synthesis of new low band gap materials. However, despite the focused effort in studying phase separation mechanism and optimum conditions to permit efficient splitting of excitons into charge carriers,[14−16,20−24] strategies to optimize film nanostructure for efficient device performance are still relatively poorly developed. It is of particular importance to understand the mechanism by which the morphology of the active layer develops during standard processing conditions. In this regard, issues of phase purity and the interdiffusion of the components are key factors that need to be considered[25−29] As such, studying the active bilayer is conceptually more straightforward.

The most widely studied donor/acceptor combination for solution processed BHJ organic solar cells is that of the donor polymer poly(3-hexylthiophene) (P3HT) and acceptor molecule [6,6] phenyl C_{61} butyric acid methylester (PCBM). In most of the reported literature bilayers are made via orthogonal solution processing, leading to some penetration of the fullerene into the underlying polymer rather than a sharp interface.[26,30−32] However, there are techniques that allow sharp interface formation including the stamp transfer printing method where films are coated into soft stamps before contact printing into the device stack.[33,34] In addition, we have also recently shown that it is possible to use a combination of solution and vacuum processing to fabricate reasonably well-defined bilayer structures of these materials.[35] Thermal annealing of such bilayers has been shown to result in diffusion of PCBM into the P3HT layer of the structure, opening up a different strategy for the control of film nanostructure.[29,34−36] We have previously used such film deposition and annealing strategies[35] in field effect transistors (FET) devices to probe the kinetics of interdiffusion of P3HT and PCBM under thermal annealing.[35] In this report, we employ photoluminescence and transient absorption spectroscopies, complimented by TEM data and KMC simulations, to correlate the different film nanostructures obtained by these fabrication procedures with exciton quenching and the kinetics of non-geminate recombination.

A schematic of the bilayer sample structure is shown in the Experimental Section. As we have shown previously, it is possible to use FET measurements to monitor the diffusion of PCBM into the polymer layer.[35,37] Following this approach, P3HT/PCBM FETs were fabricated as described in the Experimental Section; a schematic representation of the relevant device architecture is shown in the inset to Figure 1b. The bottom-contact, bottom-gate (BCBG) architecture employed here ensured that the FETs were initially solely p-type; the source-drain channel is confined to the P3HT layer[38] into which electron injection is extremely difficult and within which electron transport is negligible. Figure 1a shows the room-temperature electron field-effect mobility for bilayer P3HT:$PC_{61}BM$ and bilayer P3HT:$PC_{71}BM$ FETs, as a function of annealing temperature. Since charge-transport is known to only take place within the first few nanometres of the semiconductor-dielectric interface,[38] one can assume that when the source and drain electrodes are initially in contact with the P3HT only, injection, and transport of electrons into the device should be forbidden. By measuring the onset and magnitude of the electron mobility, information can be inferred about the resulting diffusion of PCBM to the semiconductor-dielectric interface.[35,39] The data reported in Figure 1a show that the temperature evolution of the electron mobility is similar for both P3HT/$PC_{61}BM$ and P3HT/$PC_{71}BM$ FETs, although, as discussed in detail elsewhere, the $PC_{71}BM$ devices require ≈30 °C higher temperature to initiate sufficient diffusion to register a measurable mobility.[21] It is believed that upon annealing at 120 °C for $PC_{61}BM$ and 160 °C for $PC_{71}BM$, diffusion of PCBM into the bottom P3HT layer is sufficient for percolation pathways to form at the semiconductor-dielectric interface, leading to a measurable electron mobility.[37] Upon further annealing, a drop in electron mobility is observed, which is attributed to PCBM clustering and a

dx.doi.org/10.1021/jz5018575 | J. Phys. Chem. Lett. 2014, 5, 3669−3676

reduction in two-dimensional percolation pathways. Finally, upon annealing to higher temperatures (and subsequent rapid-cooling to room-temperature) the film is believed to melt, resulting in a redistribution of the fullerene molecules and the re-establishment of percolation pathways.[39] Figure 1b shows the average hole and electron mobilities of P3HT/$PC_{71}BM$ bilayer FETs measured at room temperature after various periods of annealing at a fixed 160 °C. Based upon these studies, we selected annealing times of 30 min at 130 and 160 °C as the sample preparation conditions for our TEM and optical measurements.

Previous studies have established TEM as an effective probe of PCBM diffusion into P3HT.[27,40] Figure 2 shows typical

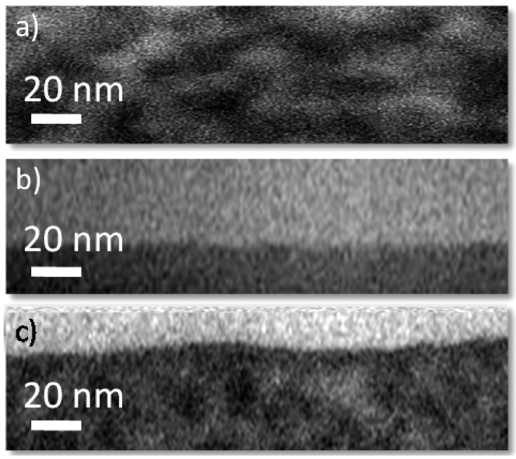

Figure 2. Cross-section TEM micrographs of (a) a not-annealed 55 nm thickness P3HT:$PC_{61}BM$ BHJ film, (b) a not-annealed P3HT (20 nm)/$PC_{61}BM$ (35 nm) bilayer sample, and (c) a 130 °C, 30 min annealed P3HT (20 nm)/$PC_{61}BM$ (35 nm) bilayer sample. The samples were prepared using focused ion beam milling and the darker regions correspond to P3HT stained with ruthenium tetroxide (RuO_4).

TEM micrographs of the cross sections of (upper panel) a not-annealed P3HT:$PC_{61}BM$ BHJ, (middle panel) a not-annealed P3HT/$PC_{61}BM$ bilayer, and (bottom panel) a 130 °C annealed P3HT/$PC_{61}BM$ bilayer film. The bilayer samples initially comprised 20 nm thickness spin-coated P3HT and 35 nm thickness evaporated $PC_{61}BM$, and the P3HT:$PC_{61}BM$ BHJ films were ~50 nm thickness. The BHJ samples present a fine degree of mixing between the P3HT and PCBM phases with the observation of some domain structure on a 10 nm length scale. In contrast, for the not-annealed bilayer, we observe a very clear and sharp interface between the two components: P3HT appears as the lower dark band and PCBM is evident as a bright layer on top. The apparent structural features here arise from the staining agent.[41] It should be noted that the observation of a sharp interface confirms that vacuum deposition of $PC_{61}BM$ onto spin coated P3HT does not cause any significant intermixing. Furthermore, we can estimate that the $PC_{61}BM$ to P3HT interface area in the not-annealed bilayer is only about 10% of that in the BHJ structure. Annealing results in an increase in the width of the dark, P3HT-containing layer and the appearance of a ~10 nm length scale domain structure, both consistent with vertical diffusion of $PC_{61}BM$ and formation of a mixed P3HT:$PC_{61}BM$ layer. The resulting nanostructure of this mixed layer is typical of that found for many conventional BHJ structured OPV blends. The remaining $PC_{61}BM$ overlayer appears largely unchanged other than having a reduced width.

The TEM micrographs and FET data were complemented by photoluminescence (PL) measurements monitoring P3HT exciton emission quenching, as shown in the Supporting Information (SI). Not-annealed P3HT:$PC_{61}BM$ BHJ films showed approximately 90% emission quenching relative to the P3HT control, consistent with previous observations.[42] Annealing of the BHJ sample results in a reduction in emission quenching, which is indicative of the formation of P3HT domains,[20] with a size that approaches the P3HT exciton diffusion length, typically estimated at 4−12 nm.[43−45] In the bilayer system, however, we observe low PL quenching (~40%) for the not-annealed structures and a significant increase in quenching upon thermal annealing (reaching ~65−80%). This is consistent with an initial layer thickness of P3HT that is greater than its exciton diffusion length and with the annealing-induced diffusion of $PC_{61}BM$ into the P3HT region causing a significant reduction in the distance over which excitons need to travel to reach a quenching donor/acceptor interface. Analogous PL quenching was observed for P3HT/$PC_{71}BM$ bilayer films (see SI).

We turn next to consideration of the influence that these different film morphologies have on charge generation and non-geminate recombination, monitored by transient absorption spectroscopy (TAS) on a microsecond time scale.[6,46] Figure 3

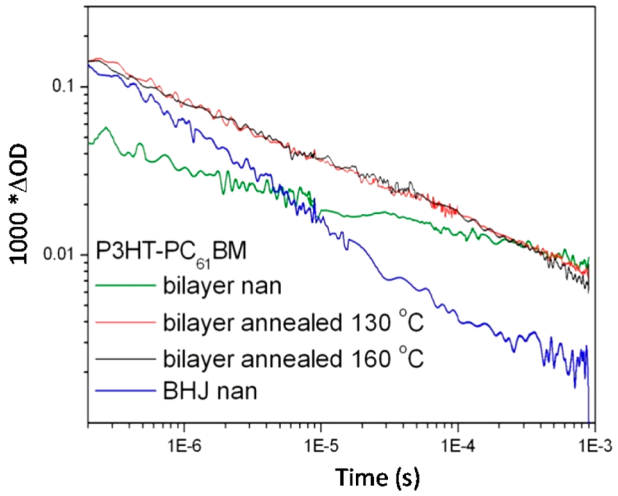

Figure 3. Transient absorption decay dynamics of P3HT:$PC_{61}BM$ BHJ and P3HT/$PC_{61}BM$ bilayer structures before and after 30 min annealing at 130 and 160 °C. Samples were pumped and probed at 520 and 980 nm, respectively, using an excitation intensity of 2 $\mu J/cm^2$.

shows the 980 nm ($P3HT^{\bullet+}$ absorption maximum[47]) TAS transients for P3HT:$PC_{61}BM$ BHJ and P3HT/$PC_{61}BM$ bilayer structures before and after 30 min annealing at 130 and 160 °C. The observed decay dynamics were oxygen-insensitive and obeyed power law characteristics, consistent with polaron rather than triplet absorption.[48] In such data, the decay dynamics is generally indicative of the rate of non-geminate recombination, while the initial amplitude is indicative of the primary yield of dissociated charges. It is apparent that the not-annealed BHJ films show a relatively high initial signal consistent with their finely dispersed nanostructure enabling efficient exciton dissociation as also concluded from the PL quenching data above. The subsequent decay is, however,

dx.doi.org/10.1021/jz5018575 | J. Phys. Chem. Lett. 2014, 5, 3669−3676

relatively rapid corresponding to a fast non-geminate recombination.[42] In the case of the not-annealed bilayer samples we observe a lower initial yield of charges, and slower recombination dynamics extending to tens of milliseconds, consistent with the spatially separated donor−acceptor nanostructure. Upon annealing these bilayer samples, the initial charge generation yield is increased to the same level as that observed for BHJ films, while the recombination dynamics show a modest acceleration to a rate intermediate between the not-annealed BHJ and bilayer films. This behavior is apparent for both $PC_{61}BM$ and $PC_{71}BM$ (see SI), although clearest for the $PC_{61}BM$-based samples shown here. We further note that, whereas the $PC_{61}BM$-based samples showed similar dynamics following annealing at either 130 or 160 °C, for $PC_{71}BM$-based samples, a higher annealing temperature is required to most closely match the not-annealed P3HT:$PC_{71}BM$ BHJ samples, consistent with the FET data we reported above.

The increase in charge generation is primarily associated with enhanced exciton dissociation at the improved D/A interfaces that result from the changes in film nanostructure (as also highlighted in the TEM and PL quenching data), modulated to some degree by the variation in P3HT ionization potential with crystallinity.[42] In particular, for the not-annealed bilayer films, the low charge generation yield and slow recombination of dissociated charges arises from the small interface area between donor and acceptor (clearly seen in the TEM data). Conversely, for the most finely mixed film, namely the BHJ sample, there is enhanced charge generation but also faster non-geminate recombination. Finally, for the annealed bilayer structure, sufficient donor/acceptor interfacial area is achieved for efficient charge generation, coupled with sufficient residual vertical segregation of polymer and fullerene to reduce non-geminate recombination, leading to a rate that is intermediate between the BHJ and not-annealed bilayer devices.

Our experimental observations (Figure 4, upper panel) indicate that the decay of charge density with time follows a power law dependence ($n(t) \propto t^{-\alpha}$), with $\alpha = 0.6$ in the case of BHJ films and $\alpha = 0.2$ for the not-annealed bilayer films. In addition, at very long times the decay in the BHJ samples undergoes a transition to an exponent of ∼0.2. While the observed changes in the yield and lifetime of charge carriers can be easily rationalized in terms of film morphology, as discussed above, the cause of the more pronounced deviation from $\alpha = 1$ bimolecular recombination[49,50] for the bilayer films is less obvious. To gain insight into this issue, we performed KMC simulations of non-geminate recombination, using a super cell containing 100 × 100 × 100 sites and assuming that electron and hole transport can be described using the Miller−Abrahams hopping rate[51] (see SI for details). The BHJ morphologies, for which one example is depicted in the upper panel inset of Figure 4, are generated using the random potential model[52] (see SI). Based on recent experimental findings for organic semiconductors,[53−56] we model the energetic disorder in bilayer and BHJ using a density of states (DoS) composed of a superposition of a Gaussian and an exponential distribution, a model that was considered previously to explain conduction in poly(arylenevinylene) light emitting diodes.[57,58] Figure 4, upper panel, compares, for BHJ films, the charge density decay dynamics deduced from TAS measurements (blue curve) with the corresponding KMC simulation data (smooth red curve). The parameters used to simulate the decay dynamics and thereby fit the experimental data are summarized in Table 1. In this table, σ_G/k_BT and σ_E/k_BT represent the width of Gaussian band and exponential band-tail states, respectively. $N_E/(N_G + N_E)$ indicates the portion of states in the exponential band-tail of DoS, and $\nu_0 \exp(-2\gamma a)$ is indicative of tunneling rate (see SI for details). As seen in the upper panel of Figure 4, the present model is able to reproduce the experimental data for the BHJ films reasonably well.

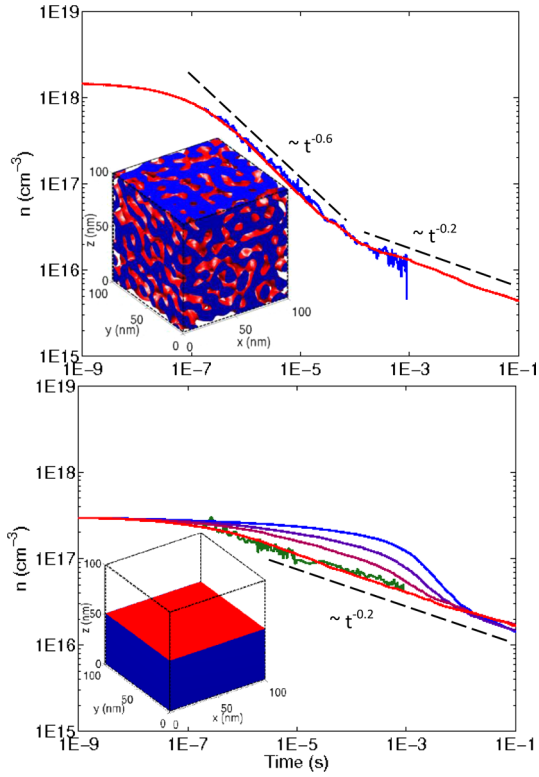

Figure 4. Upper panel compares experimental transient absorption signal data for the charge carrier density decay due to non-geminate recombination ($n(t)$) in a not-annealed P3HT/$PC_{61}BM$ BHJ thin film (blue line) with that from KMC simulations (red line). The lower panel compares transient absorption signal $n(t)$ data in a not-annealed P3HT/$PC_{61}BM$ bilayer thin film (green line) with that from KMC simulations (solid lines). The KMC results are shown for, in order of improving fit, interface confining potentials =0, 1, 2, 9 k_BT. The upper panel (lower panel) inset illustrates the KMC sample morphology used for not-annealed BHJ (bilayer) films. Power law $n(t)$ slopes are illustrated by black dashed lines with annotated exponents.

In the absence of evidence to the contrary it was decided to use the same charge carrier DoS for both the not-annealed bilayer and BHJ films. Other factors that might explain the observed recombination dynamics were then considered. The best agreement between KMC results and experiment for the bilayer films was obtained by assuming that charges reaching the interface are spatially confined to that plane, at least in the case of moderate charge densities. This behavior can result from the buildup of a potential well due to the electrostatic interaction between geminate pairs, as previously suggested for poly(p-phenylenevinylene):fullerene-derivative blend films. This potential well can result from electrostatic interactions between electrons and holes trapped at the bilayer interface.[59] Here, for the sake of simplicity, we model the potential well by lowering site energies at the interface by an amount ΔE_0 (see SI for details). Figure 4, lower panel, compares, for bilayer films, experimental data with simulation results for different values of ΔE_0; curves are shown, in order of improving fit, for $\Delta E_0 = 0$, 1,

dx.doi.org/10.1021/jz5018575 | J. Phys. Chem. Lett. 2014, 5, 3669−3676

Table 1. Best-Fit KMC Simulation Parameters for the TAS $n(t)$ Data Illustrated in Figure 4

	σ_G/k_BT	σ_E/k_BT	$N_E/(N_G+N_E)$	$\upsilon_0\exp(-2\gamma a)$ (s^{-1})	initial carrier density (cm^{-3})	$\Delta E_0/k_BT$	domain size (nm)
bilayer	3	5	1.5×10^{-3}	1E8.7	3E17	9	50
BHJ	3	5	1.5×10^{-3}	1E10.8	15E17	0	7 on average

2, and 9 k_BT. A reasonably good fit can be obtained using $\Delta E_0 \geq 3\ k_BT$ (75 meV), but the best fit is obtained for $\Delta E_0 = 9\ k_BT$ (220 meV). It is important to note that the dispersive behavior in non-geminate recombination is due to the exponential tail of DoS. Confining charges to the potential well at the interface accelerates the trapping of the charge carriers in the exponential tail. Note that if we do not include a potential well in the model, the only factor left is the morphology-dependent carrier lifetime, which results in the blue line in Figure 4 lower panel that is clearly qualitatively inconsistent with the data. The bilayer morphology used in our KMC simulations is shown in the inset within Figure 4, lower panel. As reported in Table 1, we also find that the tunneling probability (exponential prefactor, $\upsilon_0\ \exp(-2\gamma a)$; see SI for details) in the Miller-Abrahams hopping rate is about 2 orders of magnitude lower in the bilayer than in a BHJ. This can be explained by the large difference between hole and electron mobilities (see Figure 1b). In the case of BHJ films, the rate at which a hole and an electron meet depends on their mean mobility, whereas in the not-annealed bilayer films, the carriers with lower mobility (i.e., the electrons) are rate determining. Our KMC simulations show, therefore, that the difference in the non-geminate recombination dynamics observed in the BHJ and not-annealed bilayer films can be explained by a confinement of charge carriers at the two-dimensional bilayer interface that does not occur for the intercalated donor−acceptor networks in BHJ films. The effect of annealing bilayer films would then be that it disrupts the confinement potential, moving the dynamics toward those of the BHJ.

This study shows a particularly clear correlation between film structure and charge generation and recombination. One of its most striking aspects is the very large difference in non-geminate recombination induced by the difference in film nanomorphology between the bilayer and the BHJ film. We have previously reported[7] that, in agreement with the data reported here, the charge dynamics of P3HT:PCBM devices is over an order of magnitude slower in not-annealed cells than annealed cells. Numerical modeling reproduced the changes seen in the experimental data by incorporating a large change in domain size and degree of phase segregation. The annealed bilayer data we report herein infers that in addition to the spatially separated pure phase of P3HT and PCBM at the interface, there exists a second phase of amorphous, intermixed P3HT:PCBM matrix, which has resulted in an enhancement in charge generation. This is consistent with the functional model recently proposed for many organic bulk heterojunction devices by ourselves[60−62] and others.[13,36,63−65] The model is based upon charge generation within a finely intermixed polymer/fullerene phase followed by spatial separation of electrons and holes at the interface of this mixed phase with the pure/crystalline domains. Additional detailed analyses of polymer/fullerene film composition, homogeneity, phase purity and degree of crystallinity/aggregation both within and vertical to the film plane,[14,16,36,66,67] also support this argument.

In conclusion, the diffusion of PCBM in P3HT has been studied using transient absorption spectroscopy and transmission electron microscopy. P3HT:PCBM blends undergo phase-segregation upon annealing while bilayers show enhanced D/A mixing, leading to the observed transitions in photogenerated charge yields and recombination rates. Our results confirm that a key attribute of the P3HT:PCBM BHJ structure, is that it comprises both a finely mixed D/A matrix that enables efficient exciton quenching, and coexisting relatively pure domains that are effective at separating and transporting electrons and holes. Bilayer films initially show a lower recombination rates, but upon annealing the enhanced roughness increases recombination. Our study therefore demonstrates that nanomorphology, in particular, the organic−organic interfacial area, is key not only to enabling exciton quenching and the dissociation of the initially generated radical pairs, but is furthermore important in determining the efficiency of charge transport in organic solar cells and that an all optical measurement technique can be employed to study the underlying nanomorphology of different structured films.

EXPERIMENTAL SECTION

P3HT (95% regioregularity; weight-average molecular weight, $M_w \sim 60$ kg/mol) was obtained from Merck Chemicals. $PC_{61}BM$ was obtained from Solenne B.V. (>99.5% purity). Both were used as received.

Field Effect Transistor Samples. Hexamethyldisilazane (HMDS) was applied to glass substrates via vapor-phase deposition. Separate 10 mg/mL concentration solutions of P3HT and $PC_{61}BM$ were made up in chlorobenzene and left stirring overnight at 70 °C under N_2. For P3HT:PCBM blend samples, aliquots of the individual P3HT and $PC_{61}BM$ solutions were mixed in a 1:1 (wt %) ratio. The blend solutions were then deposited onto the HDMS-coated substrates via spin-coating at 1000 rpm for 60s. For bilayer samples, solutions of P3HT were first spin-coated (same conditions) onto the HDMS-coated substrates before 25 nm of PCBM was thermally evaporated (10^{-9} bar) on top at an average deposition rate of 0.3 $Å s^{-1}$, using previously reported techniques (Scheme 1).[35]

Transient Absorption Samples. Separate 10 mg/mL concentration solutions of P3HT and $PC_{61}BM$ were made up in chlorobenzene and left stirring overnight at 70 °C under N_2. For P3HT:PCBM blend samples, aliquots of the individual

Scheme 1. Schematic Diagram of P3HT/PCBM Bilayers on Glass/HMDS[a]

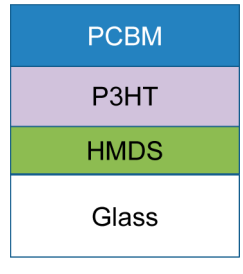

[a]The P3HT and PCBM layers were each selected to be 25 nm thickness.

dx.doi.org/10.1021/jz5018575 | J. Phys. Chem. Lett. 2014, 5, 3669−3676

P3HT and $PC_{61}BM$ solutions were mixed in a 1:1 (wt %) ratio. The blend solutions were then deposited onto the glass substrates via spin-coating at 1000 rpm for 60s. For bilayer samples, solutions of P3HT were first spin-coated (same conditions) onto the glass substrates before 25 nm of PCBM was thermally evaporated (10^{-9} bar) on top at an average deposition rate of 0.3 $Å s^{-1}$, using previously reported techniques.[35]

Transmission Electron Microscope Samples. Ten milligrams per milliliter concentration solutions of P3HT and 20 mg/mL concentration solutions $PC_{61}BM$ were made up in chlorobenzene and left stirring overnight at 70 °C under N_2. For P3HT:$PC_{61}BM$ blend samples, aliquots of the individual P3HT and $PC_{61}BM$ solutions were mixed in a 1:1 (wt %) ratio. The blend solutions were then deposited onto the glass substrates via spin-coating at 1000 rpm for 60 s. For bilayer samples, solutions of P3HT were first spin-coated (same conditions) onto the glass substrates before 35 nm of PCBM was thermally evaporated (10^{-9} bar) on top at an average deposition rate of 0.3 Å s^{-1}, using previously reported techniques.[35]

BCBG FETs were fabricated on highly doped (n^{++}) silicon wafers, which acted as the substrate and global gate electrode, with a 200 nm thermally grown silicon dioxide layer as gate dielectric. Gold source and drain electrodes were defined using standard photolithographic techniques. The silicon dioxide surfaces were then passivated with hexamethyldisilazane (HMDS). P3HT was spin-coated from 10 mg mL^{-1} chlorobenzene solutions onto the BCBG substrates. PCBM was then deposited via thermal sublimation under high vacuum (10^{-9} bar), at an average rate of 0.3 Å s^{-1}.

Transistor fabrication and electrical characterization were carried out under ambient pressure N_2 without exposure to air, using a Keithley 4200 semiconductor parameter analyzer. The mobilities of charge carriers were estimated in the saturation-regime using standard semiconductor models:[68]

$$\mu = \left(\frac{\partial\sqrt{I_D}}{\partial V_G}\right)^2 \frac{2L}{WC_i} \quad (1)$$

Here I_D is the measured drain current in the saturation regime, V_G is the applied gate voltage, L and W are the FET channel length and width, respectively, and C_i is the geometrical capacitance of the gate dielectric. The film thicknesses were measured using an Agilent 5500 atomic force microscope in tapping mode.

Transient absorption decays. Transient absorption decays were measured by exciting the sample film under a nitrogen (and oxygen) atmosphere, excitation pulses were generated with a commercially available optical parametric oscillator (Oppolette) pumped by Nd:YAG laser (Lambda Photometrics). The excitation wavelength used was 500 nm, with a pump intensity of 2 $\mu J\ cm^{-2}$ and a repetition frequency of 20 Hz. For the 1 μs to 1 ms time scale, a 100 W quartz halogen lamp (Bentham, IL 1) with a stabilized power supply (Bentham, 605) was used as a probe light source (980 nm). The signal from the photodiode was preamplified and sent to the main amplification system with an electronic band-pass filter (Costronics Electronics). The amplified signal was collected with a digital oscilloscope (Tektronics, TDS220), which was synchronized with a trigger signal of the pump laser pulse from a photodiode (Thorlabs Inc., DET210). To reduce stray light, scattered light and sample emission, two monochromators and appropriate optical cutoff filters were placed before and after the sample.

Transmission Electron Microscope Examination. Samples prepared as described above were sputtered to the desired dimensions using a focused ion beam (for cross-section) and retrieved on carbon-coated copper grids. To investigate phase segregation, the films were subject to phase contrast employing ruthenium tetroxide (RuO_4), to preferentially stain the P3HT domains. The micrographs shown in Figure 2 depict light and dark areas representing regions of PCBM and P3HT, respectively. RuO_4 staining technique has been widely used to improve image contrast in the TEM of a number of polymer and polymer blends.[69]

■ ASSOCIATED CONTENT

Ⓢ Supporting Information

Additional description of KMC Simulation and further figures on ground state absorption, photoluminescence and transient absorption decay dynamics of P3HT/$PC_{71}BM$ system are available. This material is available free of charge via the Internet at http://pubs.acs.org.

■ AUTHOR INFORMATION

Corresponding Authors

*E-mail: s.shoaee06@imperial.ac.uk.

*E-mail: j.durrant@imperial.ac.uk.

Present Address

∥(S.S.) Centre for Organic Photonics & Electronics, The University of Queensland, Brisbane, Queensland 4072, Australia.

Notes

The authors declare no competing financial interest.

■ ACKNOWLEDGMENTS

The authors are grateful to the Solvay S.A., the UK Engineering and Physical Sciences Research Council for funding this work. The work at Georgia Tech was supported by the Office of Naval Research under Grant No. N000141410171. Thanks to Ecaterina Ware for her assistance with FIB.

■ REFERENCES

(1) Forrest, S. R. The Limits to Organic Photovoltaic Cell Efficiency. *Materials Research Society Bulletin* **2005**, *30*, 28−32.

(2) Shuttle, C. G.; Hamilton, R.; O'Regan, B. C.; Nelson, J.; Durrant, J. R. Charge-Density-Based Analysis of the Current−Voltage Response of Polythiophene/Fullerene Photovoltaic Devices. *Proc. Natl. Acad. Sci. U. S. A.* **2010**, *107*, 16448−16452.

(3) Street, R. A.; Schoendorf, M. Interface State Recombination In Organic Solar Cells. *Phys. Rev. B* **2010**, *81*, 205307.

(4) Shuttle, C. G.; Regan, B. O.; Ballantyne, A. M.; Nelson, J.; Bradley, D. D. C.; Durrant, J. R. Bimolecular Recombination Losses In Polythiophene: Fullerene Solar Cells. *Phys. Rev. B: Condens. Matter Mater. Phys.* **2008**, *78*, 113201.

(5) Credgington, D.; Hamilton, R.; Atienzar, P.; Nelson, J.; Durrant, J. R. Non-Geminate Recombination as the Primary Determinant of Open-Circuit Voltage in Polythiophene:Fullerene Blend Solar Cells: An Analysis of the Influence of Device Processing Conditions. *Adv. Funct. Mater.* **2011**, *21*, 2744−2753.

(6) Shoaee, S.; Eng, M. P.; Espíldora, E.; Delgado, J. L.; Campo, B.; Martín, N.; Vanderzande, D.; Durrant, J. R. Influence of Nanoscale Phase Separation on Geminate versus Bimolecular Recombination in P3HT:Fullerene Blend Films. *Energy Environ. Sci.* **2010**, *3*, 971−976.

(7) Hamilton, R.; Shuttle, C. G.; O'Regan, B.; Hammant, T. C.; Nelson, J.; Durrant, J. R. Recombination in Annealed and Non-annealed Polythiophene/Fullerene Solar Cells: Transient Photo-

voltage Studies versus Numerical Modeling. *J. Phys. Chem. Lett.* **2010**, *1*, 1432−1436.
(8) Vandewal, K.; Tvingstedt, K.; Gadisa, A.; Inganas, O.; Manca, J. V. On the Origin of the Open-Circuit Voltage of Polymer−Fullerene Solar Cells. *Nat. Mater.* **2009**, *8*, 904−909.
(9) Scharber, M. C.; Wuhlbacher, D.; Koppe, M.; Denk, P.; Waldauf, C.; Heeger, A. J.; Brabec, C. L. Design Rules For Donors In Bulk-Heterojunction Solar Cells - Towards 10% Energy-Conversion Efficiency. *Adv. Mater.* **2006**, *18*, 789−794.
(10) Rivnay, J.; Noriega, R.; Kline, R. J.; Salleo, A.; Toney, M. F. Quantitative Analysis Of Lattice Disorder And Crystallite Size In Organic Semiconductor Thin Films. *Phys. Rev. B* **2011**, *84*, 045203.
(11) Tsoi, W. C.; James, D. T.; Kim, J. S.; Nicholson, P. G.; Murphy, C. E.; Bradley, D. D. C.; Nelson, J.; Kim, J.-S. The Nature of In-Plane Skeleton Raman Modes of P3HT and Their Correlation to the Degree of Molecular Order in P3HT:PCBM Blend Thin Films. *J. Am. Chem. Soc.* **2011**, *133*, 9834−9843.
(12) Turner, S. T.; Pingel, P.; Steyrleuthner, R.; Crossland, E. J. W.; Ludwigs, S.; Neher, D. Quantitative Analysis of Bulk Heterojunction Films Using Linear Absorption Spectroscopy and Solar Cell Performance. *Adv. Funct. Mater.* **2011**, *21*, 4640−4652.
(13) Pfannmoeller, M.; Fluegge, H.; Benner, G.; Wacker, I.; Sommer, C.; Hanselmann, M.; Schmale, S.; Schmidt, H.; Hamprecht, F. A.; Rabe, T.; et al. Visualizing a Homogeneous Blend in Bulk Heterojunction Polymer Solar Cells by Analytical Electron Microscopy. *Nano Lett.* **2011**, *11*, 3099−3107.
(14) Campoy-Quiles, M.; Ferenczi, T.; Agostinelli, T.; Etchegoin, P. G.; Kim, Y.; Anthopoulos, T. D.; Stavrinou, P. N.; Bradley, D. D. C.; Nelson, J. Morphology Evolution via Self-Organization and Lateral and Vertical Diffusion in Polymer:Fullerene Solar Cell Blends. *Nat. Mater.* **2008**, *7*, 158−164.
(15) Keivanidis, P.; Clarke, T.; Lilliu, S.; Agostinelli, T.; Macdonald, J.; Durrant, J. R.; Bradley, D. D. C.; Nelson, J. Dependence of Charge Separation Efficiency on Film Microstructure in Poly(3-hexylthiophene-2,5-diyl):[6,6]-Phenyl-C61 Butyric Acid Methyl Ester Blend Films. *J. Phys. Chem. Lett.* **2010**, *1*, 734−738.
(16) Agostinelli, T.; Lilliu, S.; Labram, J. G.; Campoy-Quiles, M.; Hampton, M.; Pires, E.; Rawle, J.; Bikondoa, O.; Bradley, D. D. C.; Anthopoulos, T. D.; Macdonald, J. E.; et al. Real-Time Investigation of Crystallization and Phase-Segregation Dynamics in P3HT:PCBM Solar Cells During Thermal Annealing. *Adv. Funct. Mater.* **2011**, *21*, 1701−1708.
(17) Xia, R.; Stavrinou, P. N.; Bradley, D. D. C.; Kim, Y. Efficient Optical Gain Media Comprising Binary Blends of Poly(3-hexylthiophene) and Poly(9,9-dioctylfluorene-*co*-benzothiadiazole). *J. Appl. Phys.* **2012**, *111*, 123107.
(18) Schueppel, R.; Schmidt, K.; Uhrich, C.; Schulze, K.; Wynands, D.; Bredas, J. L.; Brier, E.; Reinold, E.; Bu, H. B.; Baeuerle, P.; et al. Optimizing Organic Photovoltaics Using Tailored Heterojunctions: A Photoinduced Absorption Study of Oligothiophenes with Low Band Gaps. *Phys. Rev. B: Condens. Matter Mater. Phys.* **2008**, *77*, 085311.
(19) Chasteen, S. V.; Sholin, V.; Carter, S. A.; Rumbles, G. Towards Optimization of Device Performance in Conjugated Polymer Photovoltaics: Charge Generation, Transfer and Transport in Poly(*p*-phenylene-vinylene) Polymer Heterojunctions. *Sol. Energy Mater. Sol. Cells* **2008**, *92*, 651−659.
(20) Kim, Y.; Cook, S.; Tuladhar, S. M.; Choulis, S. A.; Nelson, J.; Durrant, J. R.; Bradley, D. D. C.; Giles, M.; McCulloch, I.; Ha, C.-S.; et al. A Strong Regioregularity Effect in Self-Organizing Conjugated Polymer Films and High-Efficiency Polythiophene:Fullerene Solar Cells. *Nat. Mater.* **2006**, *5*, 197−203.
(21) Peet, J.; Kim, J. Y.; Coates, N. E.; Ma, W. L.; Moses, D.; Heeger, A. J.; Bazan, G. C. Efficiency Enhancement in Low-Bandgap Polymer Solar Cells by Processing with Alkane Dithiols. *Nat. Mater.* **2007**, *6*, 497−500.
(22) Yao, Y.; Hou, J.; Xu, Z.; Li, G.; Yang, Y. Effect Of Solvent Mixture On The Nanoscale Phase Separation In Polymer Solar Cells. *Adv. Funct. Mater.* **2008**, *18*, 1783−1789.
(23) van Bavel, S. S.; Baerenklau, M.; de With, G.; Hoppe, H.; Loos, J. P3HT/PCBM Bulk Heterojunction Solar Cells: Impact of Blend Composition and 3D Morphology on Device Performance. *Adv. Funct. Mater.* **2010**, *20*, 1458−1463.
(24) Walker, B.; Tomayo, A. B.; Dang, X.-D.; Zalar, P.; Seo, J. H.; Garcia, A.; Tantiwiwat, M.; Nguyen, T.-Q. Nanoscale Phase Separation and High Photovoltaic Efficiency in Solution-Processed, Small-Molecule Bulk Heterojunction Solar Cells. *Adv. Funct. Mater.* **2009**, *19*, 3063−3069.
(25) Wang, D. H.; Lee, H. K.; Choi, D.-G.; Park, J. H.; Park, O. O. Solution-Processable Polymer Solar Cells from a Poly(3-hexylthiophene)/[6,6]-Phenyl C(61)-Butyric Acidmethyl Ester Concentration Graded Bilayers. *Appl. Phys. Lett.* **2009**, *95*, 043505.
(26) Gevaerts, V. S.; Koster, L. J. A.; Wienk, M. M.; Janssen, R. A. J. Discriminating between Bilayer and Bulk Heterojunction Polymer: Fullerene Solar Cells Using the External Quantum Efficiency. *ACS Appl. Mater. Interfaces* **2011**, *3*, 3252−3255.
(27) Chen, D.; Liu, F.; Wang, C.; Nakahara, A.; Russell, T. P. Bulk Heterojunction Photovoltaic Active Layers via Bilayer Interdiffusion. *Nano Lett.* **2011**, *11*, 2071−2078.
(28) Mueller, C.; Ferenczi, T. A. M.; Campoy-Quiles, M.; Frost, J. M.; Bradley, D. D. C.; Smith, P.; Stingelin-Stutzmann, N.; Nelson, J. Binary Organic Photovoltaic Blends: A Simple Rationale For Optimum Compositions. *Adv. Mater.* **2008**, *20*, 3510−3515.
(29) Treat, N. D.; Brady, M. A.; Smith, G.; Toney, M. F.; Kramer, E. J.; Hawker, C. J.; Chabinyc, M. L. Interdiffusion of PCBM and P3HT Reveals Miscibility in a Photovoltaically Active Blend. *Adv. Energy Mater.* **2011**, *1*, 82−89.
(30) Collins, B. A.; Tumbleston, J. R.; Ade, H. Miscibility, Crystallinity, and Phase Development in P3HT/PCBM Solar Cells: Toward an Enlightened Understanding of Device Morphology and Stability. *J. Phys. Chem. Lett.* **2011**, *2*, 3135−3145.
(31) Lee, K. H.; Schwenn, P. E.; Smith, A. R. G.; Cavaye, H.; Shaw, P. E.; James, M.; Krueger, K. B.; Gentle, I. R.; Meredith, P.; Burn, P. L. Morphology of All-Solution-Processed "Bilayer" Organic Solar Cells. *Adv. Mater.* **2010**, *23*, 766−770.
(32) Nardes, A. M.; Ayzner, A. L.; Hammond, S. R.; Ferguson, A. J.; Schwartz, B. J.; Kopidakis, N. Photoinduced Charge Carrier Generation and Decay in Sequentially Deposited Polymer/Fullerene Layers: Bulk Heterojunction vs Planar Interface. *J. Phys. Chem. C* **2012**, *116*, 7293−7305.
(33) Chen, L.; Degenaar, P.; Bradley, D. D. C. Polymer Transfer Printing: Application to Layer Coating, Pattern Definition, and Diode Dark Current Blocking. *Adv. Mater.* **2008**, *20*, 1679−1683.
(34) Ferenczi, T. A. M.; Nelson, J.; Belton, C.; Ballantyne, A. M.; Campoy-Quiles, M.; Braun, F. M.; Bradley, D. D. C. Planar Heterojunction Organic Photovoltaic Diodes via a Novel Stamp Transfer Process. *J. Phys.: Condens. Matter* **2008**, *20*, 475203.
(35) Labram, J. G.; Kirkpatrick, J.; Bradley, D. D. C.; Anthopoulos, T. D. Measurement of the Diffusivity of Fullerenes in Polymers Using Bilayer Organic Field Effect Transistors. *Phys. Rev. B* **2011**, *84*, 075344.
(36) Collins, B. A.; Gann, E.; Guignard, L.; He, X.; McNeill, C. R.; Ade, H. Molecular Miscibility of Polymer−Fullerene Blends. *J. Phys. Chem. Lett.* **2010**, *1*, 3160−3166.
(37) Labram, J. G.; Kirkpatrick, J.; Bradley, D. D. C.; Anthopoulos, T. D. Impact of Fullerene Molecular Weight on P3HT:PCBM Microstructure Studied Using Organic Field-Effect Transistors. *Adv. Energy Mater.* **2011**, *1*, 1176−1183.
(38) Horowitz, G. Organic Thin Film Transistors: From Theory to Real Devices. *J. Mater. Res.* **2004**, *19*, 1946−1962.
(39) Labram, J. G.; Domingo, E. B.; Stingelin, N.; Bradley, D. D. C.; Anthopoulos, T. D. In-Situ Monitoring of the Solid-State Microstructure Evolution of Polymer: Fullerene Blend Films Using Field-Effect Transistors. *Adv. Funct. Mater.* **2011**, *21*, 356−363.
(40) Moon, J. S.; Takacs, C. J.; Sun, Y.; Heeger, A. J. Spontaneous Formation of Bulk Heterojunction Nanostructures: Multiple Routes to Equivalent Morphologies. *Nano Lett.* **2011**, *11*, 1036−1039.

(41) Chou, T. M.; Prayoonthong, P.; Aitouchen, A.; Libera, M. Nanoscale Artifacts In RuO_4-Stained Poly(styrene). *Polymer* **2002**, *43*, 2085−2088.
(42) Clarke, T. M.; Ballantyne, A. M.; Nelson, J.; Bradley, D. D. C.; Durrant, J. R. Free Energy Control of Charge Photogeneration in Polythiophene/Fullerene Solar Cells: The Influence of Thermal Annealing on P3HT/PCBM Blends. *Adv. Funct. Mater.* **2008**, *18*, 4029−4035.
(43) Lüer, L.; Egelhaaf, H. J.; Oelkrug, D.; Cerullo, G.; Lanzani, G.; Huisman, B. H.; de Leeuw, D. Oxygen-Induced Quenching of Photoexcited States in Polythiophene Films. *Org. Electron.* **2004**, *5*, 83−89.
(44) Kroeze, J. E.; Savenije, T. J.; Vermeulen, M. J. W.; Warman, J. M. Contactless Determination of the Photoconductivity Action Spectrum, Exciton Diffusion Length, and Charge Separation Efficiency in Polythiophene-Sensitized TiO_2 Bilayers. *J. Phys. Chem. B* **2003**, *107*, 7696−7705.
(45) Shaw, P. E.; Ruseckas, A.; Samuel, I. D. W. Exciton Diffusion Measurements In Poly(3-hexylthiophene). *Adv. Mater.* **2008**, *20*, 3516−3520.
(46) Shoaee, S.; Clarke, T. M.; Huang, C.; Barlow, S.; Marder, S. R.; Heeney, M.; McCulloch, I.; Durrant, J. R. Acceptor Energy Level Control of Charge Photogeneration in Organic Donor/Acceptor Blends. *J. Am. Chem. Soc.* **2010**, *132*, 12919−12926.
(47) Korovyanko, O. J.; Österbacka, R.; Jiang, X. M.; Vardeny, Z. V.; Janssen, R. A. J. Photoexcitation Dynamics in Regioregular and Regiorandom Polythiophene Films. *Phys. Rev. B* **2001**, *64*, 235122.
(48) Montanari, I.; Nogueira, A. F.; Nelson, J.; Durrant, J. R.; Winder, C.; Loi, M. A.; Sariciftci, N. S.; Brabec, C. Transient Optical Studies of Charge Recombination Dynamics in a Polymer/Fullerene Composite at Room Temperature. *Appl. Phys. Lett.* **2002**, *81*, 3001−3003.
(49) Gillespie, D. T. Exact Stochastic Simulation of Coupled Chemical-Reactions. *J. Phys. Chem.* **1977**, *81*, 2340−2361.
(50) Gillespie, D. T. A General Method for Numerically Simulating the Stochastic Time Evolution of Coupled Chemical Reactions. *J. Comput. Phys.* **1976**, *22*, 403−434.
(51) Miller, A.; Abrahams, E. Impurity Conduction at Low Concentrations. *Phys. Rev.* **1960**, *120*, 745−755.
(52) Isichenko, M. B. Percolation, Statistical Topography, and Transport in Random-Media. *Rev. Mod. Phys.* **1992**, *64*, 961−1043.
(53) Mehraeen, S.; Coropceanu, V.; Bredas, J.-L. Role of Band States and Trap States in the Electrical Properties of Organic Semiconductors: Hopping versus Mobility Edge Model. *Phys. Rev. B* **2013**, *87*, 195209.
(54) Olthof, S.; Mehraeen, S.; Mohapatra, S. K.; Barlow, S.; Coropceanu, V.; Bredas, J.-L.; Marder, S. R.; Kahn, A. Ultralow Doping in Organic Semiconductors: Evidence of Trap Filling. *Phys. Rev. Lett.* **2012**, *109*, 176601.
(55) Zhang, Y.; de Boer, B.; Blom, P. W. M. Trap-Free Electron Transport In Poly(*p*-phenylene vinylene) by Deactivation of Traps with n-Type Doping. *Phys. Rev. B* **2010**, *81*, 085201.
(56) van Mensfoort, S. L. M.; Billen, J.; Vulto, S. I. E.; Janssen, R. A. J.; Coehoorn, R. Electron Transport in Polyfluorene-Based Sandwich-Type Devices: Quantitative Analysis of the Effects of Disorder and Electron Traps. *Phys. Rev. B* **2009**, *80*, 033202.
(57) Campbell, A. J.; Bradley, D. D. C.; Lidzey, D. G. Space-Charge Limited Conduction with Traps in Poly(phenylene vinylene) Light Emitting Diodes. *J. Appl. Phys.* **1997**, *82*, 6326−6342.
(58) Campbell, A. J.; Weaver, M. S.; Lidzey, D. G.; Bradley, D. D. C. Bulk Limited Conduction in Electroluminescent Polymer Devices. *J. Appl. Phys.* **1998**, *84*, 6737−6746.
(59) Offermans, T.; Meskers, S. C. J.; Janssen, R. A. J. Charge Recombination in a Poly(*p*-phenylene vinylene)−Fullerene Derivative Composite Film Studied by Transient, Nonresonant, Hole-Burning Spectroscopy. *J. Chem. Phys.* **2003**, *119*, 10924−10929.
(60) Jamieson, F. C.; Buchaca Domingo, E.; MaCarthy Ward, T.; Heeney, M.; Delgado, J.; Martin, N.; Stingelin, N.; Durrant, J. R. Fullerene Crystallisation as a Key Driver of Charge Separation in Polymer/Fullerene Bulk Heterojunction Solar Cells. *Chem. Sci.* **2012**, *3*, 485−492.
(61) Shoaee, S.; Subramaniyan, S.; Xin, H.; Keiderling, C.; Tuladhar, P. S.; Jamieson, F.; Jenekhe, S. A.; Durrant, J. R. Charge Photogeneration for a Series of Thiazolo-Thiazole Donor Polymers Blended with the Fullerene Electron Acceptors PCBM and ICBA. *Adv. Funct. Mater.* **2013**, *23*, 3286−3298.
(62) Westacott, P.; Tumbleston, J. R.; Shoaee, S.; Fearn, S.; Bannock, J. H.; Gilchrist, J. B.; Heutz, S.; deMello, J.; Heeney, M.; Ade, H.; et al. On the Role of Intermixed Phases in Organic Photovoltaic Blends. *Energy Environ. Sci.* **2013**, *6*, 2756−2764.
(63) Yin, W.; Dadmun, M. A New Model for the Morphology of P3HT/PCBM Organic Photovoltaics from Small-Angle Neutron Scattering: Rivers and Streams. *ACS Nano* **2011**, *5*, 4756−4768.
(64) Hopkinson, P. E.; Staniec, P. A.; Pearson, A. J.; Dunbar, A. D. F.; Wang, T.; Ryan, A. J.; Jones, R. A. L.; Lidzey, D. G.; Donald, A. M. A Phase Diagram of the P3HT:PCBM Organic Photovoltaic System: Implications for Device Processing and Performance. *Macromolecules* **2010**, *44*, 2908−2917.
(65) Wu, W.-R.; Jeng, U. S.; Su, C.-J.; Wei, K.-H.; Su, M.-S.; Chiu, M.-Y.; Chen, C.-Y.; Su, W.-B.; Su, C.-H.; Su, A.-C. Competition between Fullerene Aggregation and Poly(3-hexylthiophene) Crystallization upon Annealing of Bulk Heterojunction Solar Cells. *ACS Nano* **2011**, *5*, 6233−6243.
(66) Tsoi, W. C.; Spencer, S. J.; Yang, L.; Ballantyne, A. M.; Nicholson, P. G.; Turnbull, A.; Shard, A. G.; Murphy, C. E.; Bradley, D. D. C.; Nelson, J.; et al. Effect of Crystallization on the Electronic Energy Levels and Thin Film Morphology of P3HT:PCBM Blends. *Macromolecules* **2011**, *44*, 2944−2952.
(67) Wong, L.-Y.; Png, R.-Q.; Silva, F. B. S.; Chua, L.-L.; Repaka, D. V. M; Shi-Chen; Gao, X.-Y.; Ke, L.; Chua, S.-J.; Wee, A. T. S.; Ho, P. K. H. Interplay of Processing, Morphological Order, and Charge-Carrier Mobility in Polythiophene Thin Films Deposited by Different Methods: Comparison of Spin-Cast, Drop-Cast, and Inkjet-Printed Films. *Langmuir* **2010**, *26*, 15494−15507.
(68) Zaumseil, J.; Sirringhaus, H. Electron and Ambipolar Transport in Organic Field-Effect Transistors. *Chem. Rev.* **2007**, *107*, 1296−1323.
(69) Haubruge, H. G.; Jonas, A. M.; Legras, R. Staining of Poly(ethylene terephthalate) by Ruthenium Tetroxide. *Polymer* **2003**, *44*, 3229−3234.